

Temporal intensity correlation of light scattered by a hot atomic vapor

A. Dussaux¹, T. Passerat de Silans², W. Guerin¹,
O. Alibart³, S. Tanzilli³, F. Vakili⁴, R. Kaiser^{1*}

¹*Université de Nice Sophia Antipolis, CNRS,
Institut Non-Linéaire de Nice, F-06560 Valbonne, France*

²*Laboratório de Superfícies - DF, Universidade Federal da
Paraíba - Caixa Postal 5086, 58051-900 Joo Pessoa, PB, Brazil*

³*Université Nice Sophia Antipolis, Laboratoire de Physique de la Matière Condensée,
CNRS UMR 7336, Parc Valrose, 06108 Nice, France*

⁴*Laboratoire Lagrange, UMR 7293, Université de Nice-Sophia Antipolis (UNS),
CNRS, Observatoire de la Côte d'Azur, 06300 Nice, France*

(Dated: December 9, 2024)

Abstract

We present temporal intensity correlation measurements of light scattered by a hot atomic vapor. Clear evidence of photon bunching is shown at very short time-scales (ns) imposed by the Doppler broadening of the hot vapor. Moreover, we demonstrate that some relevant information about the scattering process, such as the ratio of single to multiple scattering, can be deduced from the measured intensity correlation function. These measurements confirm the interest of temporal intensity correlation measurements to access non-trivial spectral features, with potential applications in astrophysics.

PACS numbers:

I. Introduction

Intensity correlation was first developed in astrophysics, where the correlation of light collected by two telescopes with various separations made possible the measurement of stellar angular diameters [1] [2]. Temporal intensity correlation measurements, or intensity correlation spectroscopy, from astrophysical light sources, with a single telescope, has not been demonstrated yet due to technical challenges for the time resolution and spectral filtering, but it may be used to resolve narrow spectral features [3] [4]. On the other hand, temporal intensity correlation spectroscopy is becoming a commonly used technique in atomic physics [5] and quantum optics. Ideal photon bunching, with maximum temporal contrast, has even been recently reported in a cold-atom experiment [6]. One of the main challenge in intensity correlation measurements holds in the detection time resolution that needs to be on the order of the temporal coherence time, the latest being inversely proportional to the spectrum bandwidth. For blackbody sources, a time resolution of about 10^{-14} s is necessary [7]. Such measurements have only been achieved with two-photon absorption techniques in semiconductors [8], and in ghost imaging experiments [9]. Those are incompatible with astrophysics applications in terms of light intensity requirements. Recently, temporal photon bunching in blackbody radiation has been demonstrated with intensity correlation measurement via strong spectral filtering of the light source [10]. Here we demonstrate temporal intensity correlation measurements with a hot (room temperature and higher) atomic vapor. If our measurements from a broad pseudo-thermal source are another step towards intensity correlation spectroscopy in astrophysics, we also show that the technique can be efficiently used to measure different properties of the scattered light, such as the ratio between single and multiple scattering as a function of the optical thickness. We discuss how the time resolution as well as the complexity of the fluorescence spectrum are impacting the intensity correlation measurement. Our experimental data is compared with numerical calculations, in particular to compute the theoretical single to multiple scattering ratio and the evolution of the scattered light spectrum.

II. Experiment

In this experiment, we study the temporal intensity correlation of light scattered by a hot rubidium vapor. For a stationary process the temporal intensity correlation function is, by definition,

$$g^{(2)}(\tau) = \frac{\langle I(t)I(t+\tau) \rangle}{\langle I(t) \rangle^2} \quad (1)$$

From Cauchy-Schwarz inequalities, one can show that the $g^{(2)}(\tau)$ function is always smaller than its value at zero delay ($1 < g^{(2)}(\tau) < g^{(2)}(0)$). For chaotic light, the second order intensity correlation function can be given by the Siegert equation,

$$g^{(2)}(\tau) = 1 + \beta |g^{(1)}(\tau)|^2, \quad (2)$$

where the first order correlation $g^{(1)}(\tau)$ is the Fourier transform of the light spectrum. The factor β is linked to the number N of optical modes ($\beta = 1/N$) and denotes the spatial coherence. For a detector radius smaller than the coherence length of the scattered light, we have $\beta = 1$. In this case, and for chaotic light, the intensity correlation at zero delay is $g^{(2)}(0) = 2$ (as $g^{(1)}(0) = 1$ by definition).

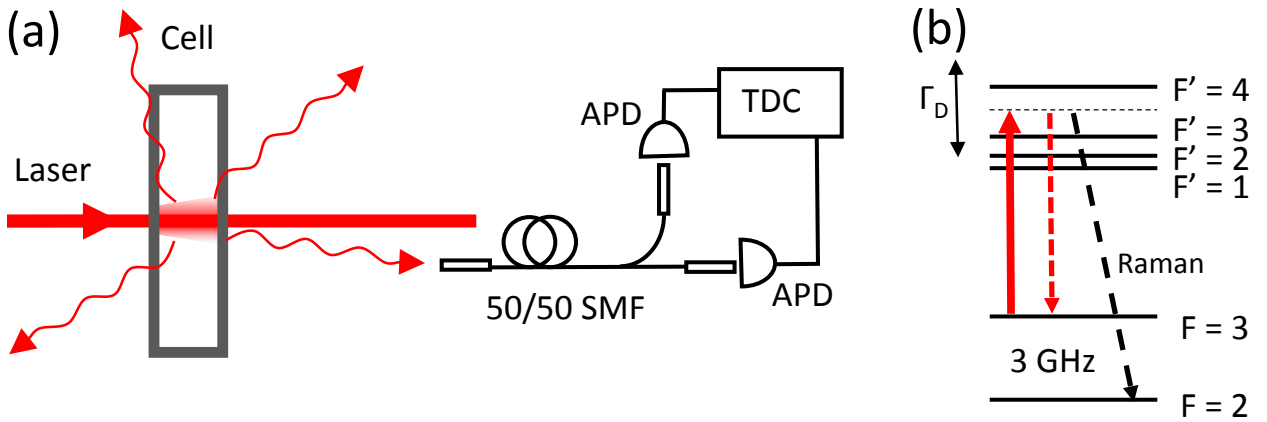


FIG. 1: (a) Experimental setup. The light scattered in the rubidium cell is collected with a nude single mode fiber beam splitter (SMF). The two outputs of the SMF beam splitter are coupled to two single photon avalanche photo diodes (APD). The photon counts are digitized with a time to digital converter (TDC) and analyzed with a computer. (b) Schematic of the Rubidium 85 D_2 transition hyperfine structure. (red arrows) Excitation and emission at the $\{F = 3 \rightarrow F' = 3, F = 3 \rightarrow F' = 4\}$ crossover frequency. Γ_D gives the magnitude of the Doppler broadening. (black dashed arrow) Emission through Raman scattering.

In the present experiment, we used a rubidium cell, with a natural mixture of the isotopes, with a radius of 10 cm and a thickness of 5 mm (see Fig.1 a). The beam of a commercial

extended cavity laser diode was centered in the middle of the cell with a waist of 2 mm and a power of 900 μW . The scattered light was collected with a single mode fiber, placed at a distance $L = 25\text{cm}$ after the cell, with an angle $\theta = 5.6^\circ$ from the laser propagation direction, without any coupling lens. The distance was chosen to make sure that the conditions for maximum spatial coherence ($\beta = 1$) were satisfied [6]. Indeed, the correlation length was estimated to be $l_c = \lambda L / (\pi s) = 62\mu m$ for a source radius $s = 1\text{mm}$, which is much larger than the mono-mode fiber mode-field diameter ($\approx 5 - 6\mu m$). The coupled light was split with a 50/50 fibered beam splitter and detected by two single-photon avalanche photo-diodes (model SPCM-AQRH from Excelitas Technologies [11]) with a quantum efficiency of about 60 % at 780 nm. To build up the $g^{(2)}(\tau)$ measurements, time tags, with a resolution of 160 ps, were obtained from a multichannel time to digital converter, and sent for analysis to a computer. For the measurements presented here, the laser frequency was locked at the $\{F = 3 \rightarrow F' = 3, F = 3 \rightarrow F' = 4\}$ cross over frequency of the rubidium 85 D_2 line. The rubidium cell was placed in an oven in order to vary the saturation vapor pressure and therefore the atomic density. The temperature was varied from 20° C to 78° C, leading to optical thicknesses b in the range $0.07 < b < 12$. The detector count rate was ranging between $2.7 \times 10^3 s^{-1}$ and $4 \times 10^4 s^{-1}$. In order to keep the signal high compared to stray light and detector dark counts, decision was made to not use a polarizer after the rubidium cell, mainly due to the low count rate at the lowest temperatures/optical thickness. The measurement time, from 10 hours to a couple of days, was adapted to observe a total number of counts of at least 5×10^8 for every series of measurements. The temperature of the cell was obtained by fitting the transmission through the cell as a function of the laser frequency, with low power [12], in the full range of the rubidium 85 and 87 D_2 lines. Even though this was not a critical parameter in the work presented here, a good precision on the temperature was obtained by simultaneously fitting the Doppler broadening of the rubidium multilevel cross-section and the temperature-dependent atomic density (through the optical opacity).

III. Results

In Fig.2 a, we show, as an example, the intensity correlation measured for $b = 0.38$. At first, we clearly see the modification of the photon statistics induced by the scattering of the light by the atoms. This evidence of photon bunching was indeed not observed with the light scattered by a piece of white paper. We also see that the ideal value $g^{(2)}(0) = 2$ is not reached and that the correlation decay cannot be described with a simple Gaussian

function. In order to compare the measurements made at the different optical thicknesses, we normalized the $g^{(2)}(\tau) - 1$ curves by the temporal contrast defined as $g^{(2)}(0) - 1$, the resulting intensity correlations are shown in Fig.2 b) (dots). From here, the shape of the measured intensity correlation and the evolution of the temporal contrast (Fig. 5 b) will be discussed separately. The measured correlation clearly reveal the superposition, with various weights, of sensitively different decay times. At large optical depths, the scattered light measured in transmission is mainly composed of photons that have scattered more than once. The Doppler broadening of the scattered light is in average isotropic and one expects a complete frequency redistribution (CFR) [13]. Fitting the $g^{(2)}(\tau)$ curve obtained for $b = 4$ with a Gaussian distribution gives a Doppler width of $2\pi.212$ MHz (pink line) which is close to the Doppler width expected in the CFR regime at 64°C , $\sigma_m = \sqrt{\frac{k_B T}{mc^2}} \omega_0 = 2\pi.230$ MHz, with ω_0 the atomic transition angular frequency, k_B the Boltzman constant, T the temperature, m the mass of the rubidium atoms and c the speed of light. For a small optical thickness, most of the detected photons only scattered once. There, the Doppler broadening is anisotropic and we expect it to be $\sigma_s = \sin\theta .\sigma_m = 2\pi.21$ MHz in the single scattering regime at $T = 20^\circ\text{C}$, with $\theta = 5.6^\circ$ the measured angle between the detector axis and the laser propagation direction. This is in good agreement with the 23 MHz value measured for our smallest optical thickness $b = 0.076$. From here, we will show that temporal intensity correlation measurement can be used for a quantitative measurement of the multiple scattering ratio.

In the intermediate regime between single and multiple scattering, the Doppler-broadened spectra can be approximated by:

$$P(\omega) \propto a \exp\left(-\frac{(\omega - \omega_0)^2}{2\sigma_m^2}\right) + b \exp\left(-\frac{(\omega - \omega_0)^2}{2\sigma_s^2}\right) \quad (3)$$

with a and b the relative amplitudes of the two components ($a + b = 1$). With this definition, the ratios of multiple and single scattering (proportional to the area of each Gaussian) are $R_m = a\sigma_m/(a\sigma_m + b\sigma_s)$ and $R_s = b\sigma_s/(a\sigma_m + b\sigma_s)$. This leads to the temporal intensity correlation,

$$g^{(2)}(\tau) - 1 = R_m^2 e^{(-\sigma_m^2 \tau^2)} + R_s^2 e^{(-\sigma_s^2 \tau^2)} + 2R_m R_s e^{(-\sigma_m \sigma_s \tau^2/2)} \quad (4)$$

Note that, as $g^{(2)}(\tau)$ is a quadratic function of $g^{(1)}(\tau)$, the two components of the optical

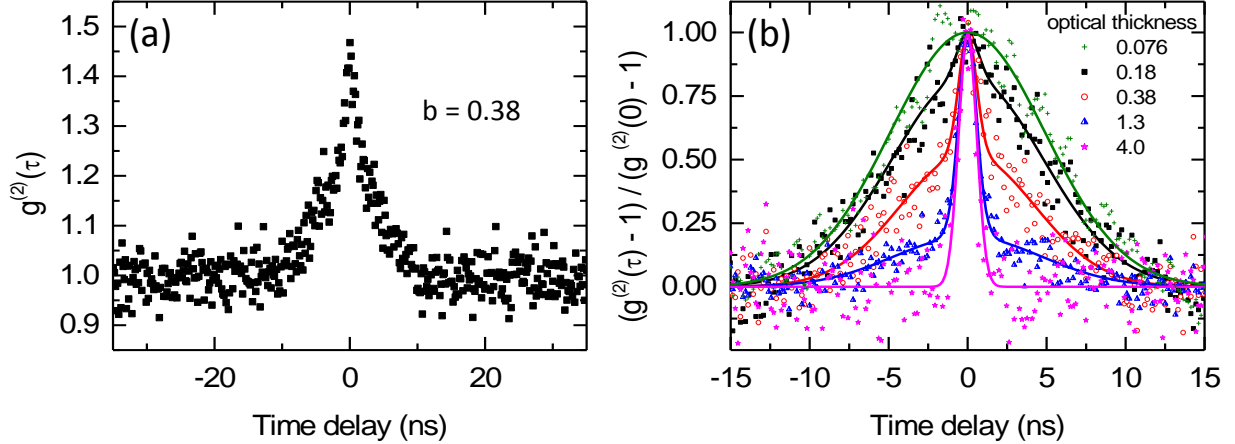


FIG. 2: (a) Measurement of the second order intensity correlation $g^{(2)}(\tau) - 1$ as a function of the time delay. (b) Experimental data normalized by the contrast (dots). Numerical fit according to Eq. 4, with the ratio σ_m/σ_s fixed by the experimental measurement of the detector position (full lines).

spectrum give rise to the superposition of three decay times. Fig.2 b) shows the fit of the measured $g^{(2)}(\tau)$ by Eq.4 (full lines), with all parameters set free, apart from the ratio $\sigma_s/\sigma_m = \sin\theta$, fixed according to the experimental detection angle. The calculated fits as well as the experimental data have been normalized by the contrast ($R_m^2 + R_s^2 + R_m R_s$) shown in Fig. 5 b) (black squares). On Fig. 3 b), we show the deduced single scattering ratio R_s as a function of the optical thickness.

We also performed measurement while detuning the laser frequency out of the atomic resonance with a fixed atomic density (green dots). For detunings smaller than the Doppler width Γ_D , this mainly acts as a change of the optical thickness. The shift of the central frequency of the spectrum [14] does not affect the $g^{(2)}(\tau)$ curve according to Eq. 4. For larger detunings, two asymmetric components are expected in the spectrum [14], this goes beyond our simple model and may not be resolved with our experimental time resolution and signal to noise.

IV. Simulations

In order to determine the accuracy of this measurement, we performed random walk simulations with a Monte Carlo routine based on first principles. The simulations use a two-

level atom model. The absorption profile of the vapor is a Voigt profile (velocity integration):

$$\alpha(\omega) \propto \int dv e^{-v^2} \frac{1}{1 + 4\frac{\omega^2}{a^2}} \quad (5)$$

with $a = \Gamma/\Gamma_D$, where Γ is the natural line width, $\Gamma_D = 2u/\lambda$ is the Doppler width at $1/e$ of its maximum, $u = \sqrt{2k_B T/m}$ is the half-width of the Maxwell-Boltzmann velocity distribution, λ is the wavelength of the atomic transition. The detuning ω is taken in units of Doppler width, we have $u = 1$ and $\lambda = 1$ such that $\Gamma_D = u/\lambda = 1$. A cell with the same dimensions of the cell of the experiment is considered (radius 10 cm thickness 5mm). The incident beam is infinitely narrow, it is centered and spectrally monochromatic. By computing the path and the Doppler frequency shift of a large number of photons, we are able to build up statistics about the number of scattering events and frequency distribution of the output photons. In Fig. 3 b) we show, for different values of optical thicknesses, the probability that a photon, initially at resonance, and detected in the solid angle $0^\circ < \theta < 5^\circ$, has scattered n times. The solid angle was chosen larger than in the experiment in order to reduce the computing time. The data shown here was not very sensitive to this angle, especially at small optical thickness. The deduced values of single scattering ratio ($n = 1$) are summarized in Fig. 3 b) (red squares). We can see that the ratio deduced with our experimental measurement and our simple model is well reproduced by the simulations.

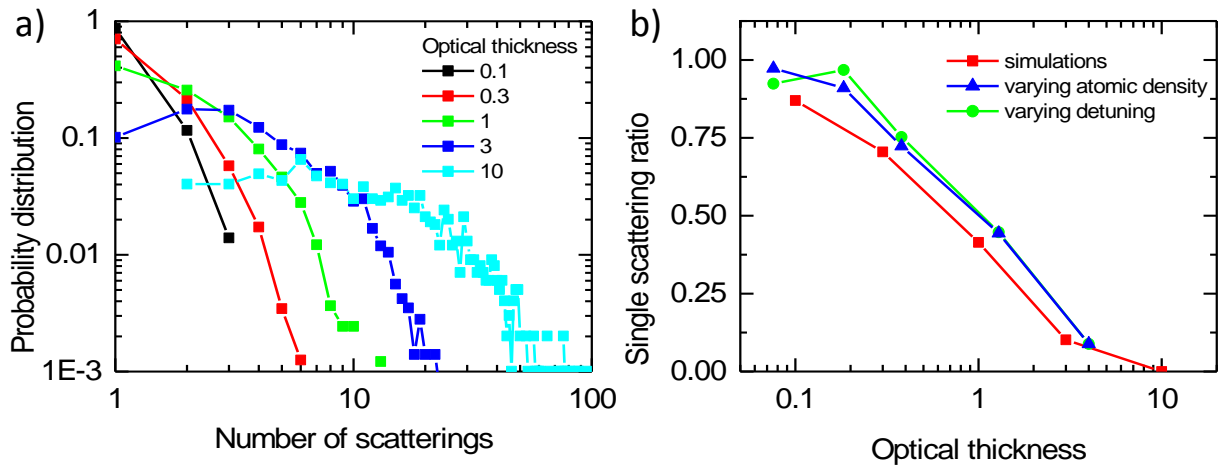


FIG. 3: (a) Simulated probability that a photon detected in the solid angle $0^\circ < \theta < 5^\circ$ has scattered n times. (b) Single scattering ratio R_s as a function of the optical thickness.

It must be stressed that the simulations do not take the multilevel structure of rubidium into account, neither non elastic scattering such as Raman scattering or the Mollow triplet

[15]. In contrast with intensity correlation measurements with cold atoms, the Mollow triplet is expected, here, to give rise to a decay time on much longer time scale (μs scale) than the Doppler broadening. Furthermore, the applied laser intensity of about 10 times the saturation intensity is only expected to induce a saturation of the atoms with a small longitudinal velocity and in the center of the laser beam. None of the measurements revealed such a slow decay time.

On the other hand, anti-Stokes Raman scattering between the ground levels ($F = 3 \rightarrow F = 2$) may not be negligible (see black dashed arrow in Fig.1 b)). In Fig. 4 a), we show the evolution of the emission spectrum of rubidium at room temperature by taking the multilevel structure and the Raman scattering into account. The spectra are calculated for an infinite medium by including the laser spectral width, the frequency dependent atomic cross-section, the Maxwell-Boltzman distribution of the atomic velocities and the different transition factors within the multilevel structure. The numerical method used for single and multiple scattering is detailed in [16] (see equations 19 and 21). We used, as in the experiment, a 1 MHz broad excitation at the Rubidium 85 crossover frequency. For the spectrum after the first scattering we considered two cases. First, an emission at $\theta = 90^\circ$ which gives a good estimation of the spectrum averaged in all the scattering angles (red curve Fig. 4 b)). This is necessary to calculate the next spectra [16] but does not reflect the spectrum measured in our experiment. In order to simulate the single scattering spectrum as measured in the experiment, we include the angle dependence by considering the energy conservation of a photon scattered at $\theta = 5.6^\circ$ from the incident laser propagation direction (see black curve in Fig. 4 b)) [23]. For the multiple scattering regime, we calculated the evolution of the spectra after up to 10 scattering events which was enough to obtain a complete frequency redistribution (no noticeable change of Raman scattering ratio, neither change of the spectrum linewidth was observed above).

V. Discussion

In order to determine the impact of the multilevel structure of the rubidium and the Raman scattering on our intensity correlation measurement, we estimated the spectrum of the measured photons as a function of the optical thickness by multiplying the spectra shown in Fig. 4 a) with their respective weights as given in Fig. 3 a). As an example, we show the theoretical correlation for $b = 10$ on Fig. 5 a) (black curve).

By itself, the impact of the hyperfine structure of the excited states only gives rise to

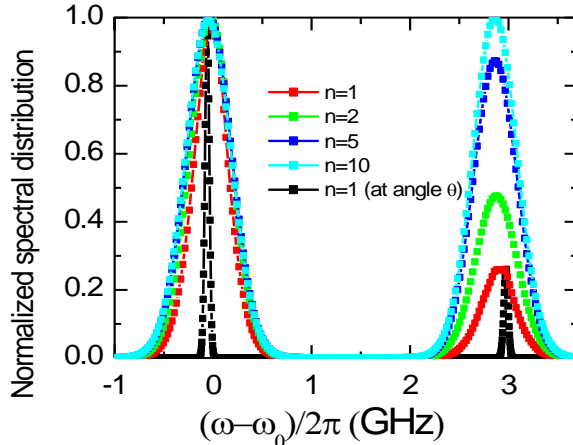


FIG. 4: Simulated evolution of the emission spectrum, averaged in all directions at room temperature, by taking the multilevel structure and the Raman scattering into account. (black curve) Spectrum after the first scattering for $\theta = 5.6^\circ$

a larger effective broadening of the spectrum. This induces a negligible decrease of the correlation decay time. To the contrary, we calculate that 26% of the photons are scattered through Raman scattering at the first scattering event. This ratio increases with the number of scattering events (up to $\approx 50\%$). One of the consequences is a small decrease of the overall atomic cross section σ_{sc} that is not included in the random walk simulations.

The main impact of the Raman scattering on our measurement, is the beating at 3 GHz between the Rayleigh and the Raman components of the fluorescence spectrum. This results in an oscillatory behavior of the intensity correlation, on a timescale that is not accessible with our experimental setup. In Fig. 5 a) we show, as an example, the calculated $g^{(2)}(\tau)$ curve for $b = 10$ (black line) where we can consider a complete frequency redistribution. We then calculate the convolution between $g^{(2)}(\tau)$ and a Gaussian function of FWHM = 350 ps (grey dashed line) to simulate our detector jitter (red line) [11]. The red squares simulate the time binning (160 ps) imposed by the time to digital converter. If the timing resolution suppresses the oscillations, it also induces a reduction of the measured contrast, proportional to the Raman scattering rate. Fig. 5 b) shows the resulting contrast for the calculated $g^{(2)}(\tau)$ (green triangles) and the contrast of the measured $g^{(2)}(\tau)$ (black squares). The calculated contrast has also been divided by a factor two to account for the fact that no polarizer was placed between the cell and the detector [17] during the experiment (red dots). Note that

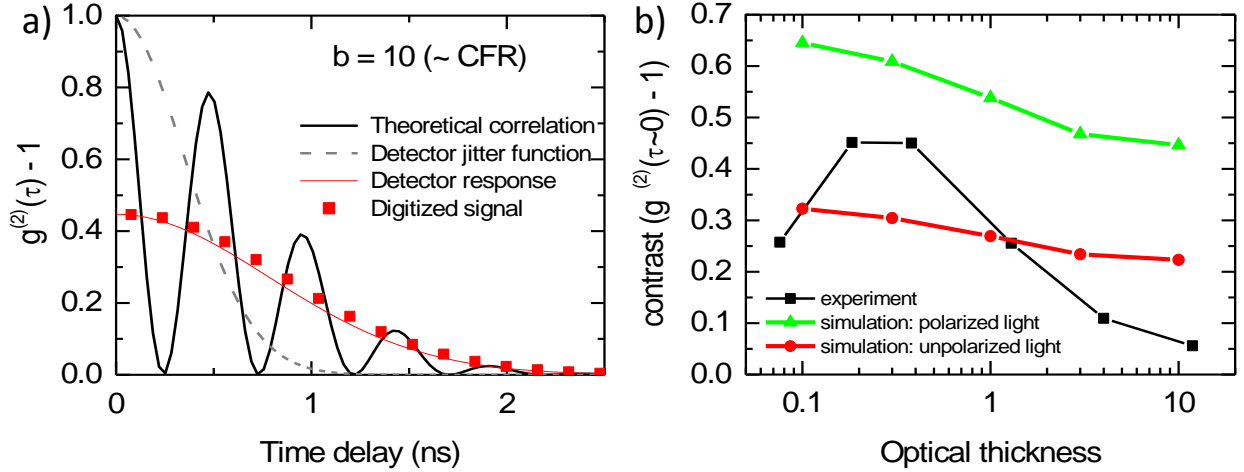


FIG. 5: a) (black line) Calculated $g^{(2)}(\tau)$ curve for $b = 10$, (grey dashed line) 350 ps detector jitter, (red line) convolution between $g^{(2)}(\tau)$ and the detector jitter, (red squares) simulation of the signal as given by the time to digital converter. b) (black squares) Contrast of the experimental measurement. Simulated contrast for a fully polarized light (green triangles), unpolarized light (red dots).

additional measurements with a faster detector (70 ps jitter) but lower quantum efficiency revealed the $g^{(2)}(\tau)$ oscillation due to Raman scattering (not shown). The experimental signal to noise ratio did not allow us to make any quantitative measurement of the Raman scattering rate.

The normalized $g^{(2)}(\tau)$ curves calculated for the different values of optical thickness, including the multilevel structure, the Raman scattering, and the detection time resolution are shown in Fig. 6. The single scattering and CFR regimes are respectively calculated from the spectra after $n = 1$ and $n = 10$ scatterings. Despite the presence of non-elastic scattering and the complex multilevel structure of rubidium, we can see a very good agreement between the simulated and measured $g^{(2)}(\tau)$ curves (Fig. 2 b). The analysis of the measured contrast still shows some unexplained features. Apart for the smallest optical thickness $b = 0.07$, the level of stray light was very low compared to the atomic fluorescence and one would expect the contrast to follow the behavior shown by the red dots on Fig.5 a). We believe that the higher contrast observed for $b < 1$ is due to a high remaining polarization of the scattered photons. This could be verified in further experiments with the use of a polarizer before the detector. Even though the light is expected to be fully depolarized after a high number of

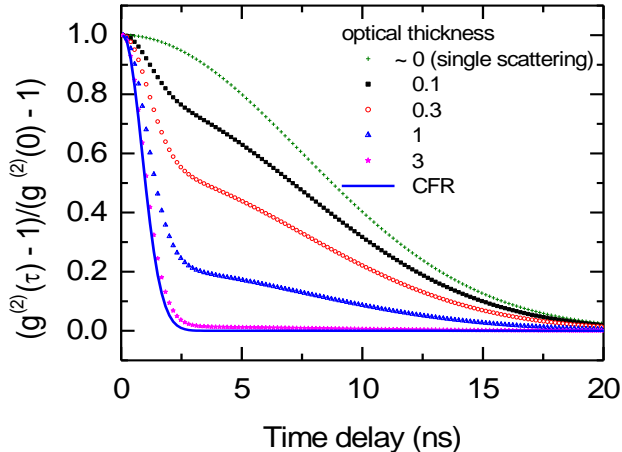


FIG. 6: Simulation of the second order intensity correlation $g^{(2)}(\tau) - 1$ as a function of the time delay for different optical thicknesses, by taking the detector jitter and time resolution into account. The single scattering and CFR regimes are respectively calculated from the spectra after $n = 1$ and $n = 10$ scatterings. The data has been normalized by the contrast shown in Fig. 5 b)

scattering events, the contrast decreases faster than expected as the high optical thicknesses increases. It should be mentioned that the same phenomena has been predicted [18] and observed in a cold atom experiment [19] where radiation trapping (with optical thicknesses as low as 0.4) was considered as the origin of the $g^{(2)}(0)$ decay. Nevertheless, this assumption was contradicted in a more recent publication, where full contrast intensity correlation was reported in optical molasses with an optical density going up to 3 [6]. Further measurements with a polarizer would, again, allow us to discard the impact of the fluorescence polarization in order to get a better understanding of this phenomena. Ultra narrow spectral filtering could also be used to isolate the Rayleigh component of the spectrum and cancel the $g^2(\tau)$ oscillations caused by Raman scattering. We already checked that the stray light (e.g. from the laser diode amplified spontaneous emission), or the level of fluorescence, as well as the increase of the source size with b due to diffusion [20], are not responsible for the anomalous decrease of contrast.

VI. Conclusion

Intensity correlation measurements with broadband light is challenging as it requires a detection with a high time resolution. Here we have demonstrated intensity correlation with a hot atomic vapor where the coherence time is much lower than with cold atoms. This goes toward applications to astrophysics where sub-GHz spectral filtering is still challenging in

the visible range [21] and where spectral features such as astrophysics lasers may be investigated [3] [4]. We have shown that we were able to quantitatively measure single to multiple scattering ratio by demonstrating a good agreement between experimental and simulated results. These measurements may also be useful, in further studies, to investigate the polarization or the anomalous correlation of the scattered light at different optical thicknesses. In particular, it is still not clear why the contrast is reduced at high optical thicknesses. One may also question the impact of the non-Gaussian statistics of the photon step length in atomic vapors [22].

Acknowledgments

A.D. is supported by Campus France (Program n.CF-PRESTIGE-18-2015).

* Electronic address: antoine.dussaux@inln.cnrs.fr

- [1] R. Hanbury Brown and R. Q. Twiss, *Nature* **178**, 1046 (1956).
- [2] R. Hanbury Brown, *Nature* **218**, 637 (1968).
- [3] S. Johansson and V. Letokhov, *New Astronomy* **10**, 361 (2005).
- [4] D. Dravins and C. Germanà, in *AIP Conference Proceedings*, edited by O. Ryan and A. Shearer (American Institute of Physics, ADDRESS, 2008), Vol. 984, pp. 216–224.
- [5] C. Jurczak *et al.*, *Optics Communications* **115**, 480 (1995).
- [6] K. Nakayama *et al.*, *Opt. Express* **18**, 6604 (2010).
- [7] C. Mehta, *Il Nuovo Cimento (1955-1965)* **28**, 401 (1963).
- [8] F. Boitier *et al.*, *Nat Phys* **5**, 267 (2009).
- [9] S. Karmakar, R. Meyers, and Y. Shih, *Proc. SPIE* **8518**, 851805 (2012).
- [10] P. K. Tan *et al.*, *The Astrophysical Journal Letters* **789**, L10 (2014).
- [11] E. Technologies, SPCM-AQRH Single Photon Counting Module, http://www.excelitas.com/Downloads/DTS_SPCM-AQRH.pdf.
- [12] A. Millett-Sikking *et al.*, *Journal of Physics B: Atomic, Molecular and Optical Physics* **40**, 187 (2007).
- [13] A. F. Molisch and B. P. Oehry, Oxford University Press (1998).
- [14] J. C. A. Carvalho *et al.*, *Phys. Rev. A* **91**, 053846 (2015).
- [15] B. R. Mollow, *Phys. Rev.* **188**, 1969 (1969).

- [16] N. Mercadier *et al.*, Phys. Rev. A **87**, 063837 (2013).
- [17] R. Hanbury Brown, London: Taylor & Francis (1974).
- [18] M. Beeler *et al.*, Phys. Rev. A **68**, 013411 (2003).
- [19] R. Stites *et al.*, Opt. Lett. **29**, 2713 (2004).
- [20] Q. Baudouin *et al.*, Phys. Rev. E **90**, 052114 (2014).
- [21] P. K. Tan *et al.*, The Astrophysical Journal Letters **789**, L10 (2014).
- [22] N. Mercadier *et al.*, Nat Phys **5**, 602 (2009).
- [23] From equation 19 in [16], we replace v_x and v_y by $\sin\theta v_x$ and $(1 - \cos\theta)v_y$ in the Dirac distribution that denotes the energy conservation.